# Stability of developing film flow down an inclined surface

Sarath Ramadurgam, R. V. K. Chakravarthy, Gaurav Tomar, and Rama Govindarajan

## Related Articles

## Additional information on Phys. Fluids

# Stability of developing film flow down an inclined surface

Sarath Ramadurgam,[1] R. V. K. Chakravarthy,[2] Gaurav Tomar,[3]
and Rama Govindarajan[4,a)]

[1]*Department of Physics, Purdue University, West Lafayette, Indiana 47907, USA*
[2]*Department of Aerospace Engineering, Indian Institute of Technology Madras,*
*Chennai 600036, India*
[3]*Department of Mechanical Engineering, Indian Institute of Science,*
*Bangalore 560012, India*
[4]*TIFR Centre for Interdisciplinary Sciences, Tata Institute of Fundamental Research,*
*Hyderabad 500075, India*

Film flows on inclined surfaces are often assumed to be of constant thickness, which ensures that the velocity profile is half-Poiseuille. It is shown here that by shallow water theory, only flows in a portion of Reynolds number-Froude number ($Re$–$Fr$) plane can asymptotically attain constant film thickness. In another portion on the plane, the constant thickness solution appears as an unstable fixed point, while in other regions the film thickness seems to asymptote to a positive slope. Our simulations of the Navier-Stokes equations confirm the predictions of shallow water theory at higher Froude numbers, but disagree with them at lower Froude numbers. We show that different regimes of film flow show completely different stability behaviour from that predicted earlier. Supercritical decelerating flows are shown to be always unstable, whereas accelerating flows become unstable *below* a certain Reynolds number for a given Froude number. Subcritical flows on the other hand are shown to be unstable above a certain Reynolds number. In some range of parameters, two solutions for the base flow exist, and the attached profile is found to be more stable. All flows except those with separation become more stable as they proceed downstream. © *2012 American Institute of Physics*. [http://dx.doi.org/10.1063/1.4758299]

## I. INTRODUCTION

Film flows down an incline exhibit a plethora of complex dynamics which are of relevance in geophysical situations as well as in engineering processes, see, e.g., Refs. 1 and 2. Studies on the stability of laminar film flows comprise too large a volume of literature to recount here, and excellent overviews are available, for example in Ref. 3, so only a few are mentioned. The earliest analytical studies of the linear stability of thin film flows were carried out by Benjamin[4] and Yih[5] where the Orr-Sommerfeld equation was solved analytically for long-wavelength perturbations and small Reynolds number flows. These studies were extended to higher Reynolds number flows in Refs. 6 and 7 among others. The effect of surface tension was studied by Ref. 8. At finite wavelengths, the linear stability may be decided by the solution of a quadratic eigenvalue problem, solved for example in Ref. 9. Benney,[10] who was the first to derive a nonlinear equation of evolution for the film interface of an isothermal laminar flow down an inclined plane,[11] experimentally showed that at low angles the onset of instability follows Yih's result. A detailed numerical study of the propagation of waves in thin films was done in Ref. 3. They obtain good agreement in certain cases with the experiments of Ref. 11. More recently in Ref. 12 the complete Navier-Stokes equations (NSEs) were solved to obtain the base flow in the nonlinear wavy regime.

---

a)On lien from the Jawaharlal Nehru Centre for Advanced Scientific Research, Bangalore 560064, India. Electronic mail: rama@tifrh.res.in.

Most of the earlier instability work on thin film flows have assumed parallel flow with half-Poiseuille velocity profile or a higher order polynomial function.[4-6] The present work differs from these in a significant respect: under shallow water theory (SWT) we study analytically the stability of the region where the base flow evolves with downstream distance $x$. We show that the basic flow has a richer structure than elucidated earlier, with interesting consequences for stability. It is further shown that the parabolic velocity profile despite being a valid solution is not displayed over long downstream distances. The recent experimental work of Ref. 13 shows evidence for velocity profiles which are not parabolic. We also study the problem numerically by solving the Navier-Stokes equation for an inclined film flow. The simulations confirm the predictions of shallow water theory at higher Froude numbers, both in terms of evolution of the film thickness, and in finding non-parabolic velocity profiles over long streamwise distances. In particular, the switch at a particular Reynolds number, between two kinds of solutions is found in both Navier-Stokes simulations and SWT. At low Froude numbers, we find a qualitative difference between Navier-Stokes and SWT.

At higher Froude numbers, the fact that a long stretches of the film do not display a parabolic velocity profile indicates that stability of developing profiles must be studied to predict whether a steady laminar parabolic profile will be attained. The recent work of Refs. 14 and 15 do study the stability of developing profiles, but are not as general as the work. In Ref. 14, the stability of the developing profile of a high Reynolds number and high surface tension Nusselt flow along a vertical plane is studied. In Ref. 15, a model is used for the skin friction, which dictates downstream development in the high Froude number flow considered.

The shallow water equations for film flows on inclined surfaces are transformed in Sec. II A into variables convenient for obtaining solutions, and the solution approach followed in Ref. 16 is used to obtain the basic flow according to SWT. The basic flow is predicted to belong to four branches, depending on the Reynolds number $Re$ and the initial Froude number $Fr_i$, revealing a richer structure than known before. In Sec. II B we compare the predictions of shallow water theory to numerical simulations of the Navier-Stokes equation. The linear stability of film flows of the various types is studied in Sec. III, and found to be completely different on different regions of the $Re$–$Fr$ plane.

## II. THE BASIC FLOW

Consider two-dimensional film flow along a flat plate held at an inclination of $\theta$ with respect to the horizontal. The continuity and momentum equations that govern the flow are

$$\nabla \cdot \mathbf{u} = 0 \tag{1}$$

and

$$\frac{\partial u}{\partial t} + \mathbf{u} \cdot \nabla \mathbf{u} = -\frac{1}{\rho}\nabla p + \nu \nabla^2 \mathbf{u} + g\mathbf{z} + \frac{\sigma}{\rho}\nabla\left[\frac{\nabla^2 h}{(1+h'^2)^{3/2}}\right], \tag{2}$$

respectively. Here $\mathbf{u}$ is the velocity vector, $u$ and $v$ being its coordinates along the direction $x$ parallel to the flat plate, and the wall normal direction $y$, respectively, $p$ is the pressure, $g$ is the acceleration due to gravity, $\rho$, $\nu$, and $\sigma$, respectively, are the density, kinematic viscosity, and surface tension of the fluid, $h(x)$ is the height of the fluid film, $\mathbf{z}$ is a unit vector in the vertical direction, and $t$ is the time. The prime on $h$ refers to a derivative with respect to $x$. At each $x$, global continuity dictates that

$$Q = \int_0^{h(x)} u(y)dy \tag{3}$$

is satisfied, where $Q$ is the constant volumetric flow rate. The equations may be non-dimensionalised by using the local height $h$, and the average film velocity $U = Q/h$ as the length and velocity scales, respectively. The momentum equation may then be written as

$$\frac{\partial u}{\partial t} + \mathbf{u} \cdot \nabla \mathbf{u} = -\nabla p + \frac{1}{Re}\nabla^2 \mathbf{u} + \frac{\sec\theta\,\mathbf{z}}{Fr^2} + \frac{h^2}{We}\nabla\left[\frac{\nabla^2 h}{(1+h'^2)^{3/2}}\right]. \tag{4}$$

The dimensionless parameters in the problem thus are the Reynolds number $Re \equiv Q/\nu$, the Froude number $Fr \equiv U/(g\cos\theta h)^{1/2}$, and the Weber number $We = \rho U^2 h/\sigma$. This definition of Froude number is not valid at $\theta = 90°$ as it renders the governing Eq. (4) indeterminate. However, this non-dimensionalisation is appropriate for the present study, since it is limited to small angles of inclination. Further, note that the Reynolds number is constant for a given flow and the adoption of local scales entails a change of coordinate system from $(x, y)$ to $(\zeta, \eta)$, where $d\zeta = dx/h(x)$, and $\eta = y/h(x)$.

## A. Shallow water theory

In order to reduce Eq. (4) to the steady boundary layer shallow water equation (BLSWE), we set the time derivative to 0, and make the shallow water approximation of a slow variation in *x*. This means we may neglect all except the first derivative in *x* or $\zeta$, except in the numerator of the surface tension term, since this term can become large for small Weber number. Further, from the continuity equation the velocity may be expressed in terms of the basic streamfunction $\Psi = Qf(\eta, \zeta)$ as

$$\bar{u} = \frac{Q}{h} f_\eta, \quad \bar{v} = \frac{Q}{h} \left( \eta h' f_\eta - f_\zeta \right). \tag{5}$$

The overbars refer to mean quantities. In the transformed coordinate system, we then arrive at the weakly non-similar BLSWE for flow along an incline:

$$\frac{1}{Re} f_{\eta\eta\eta} - \frac{1}{Fr^2} \left( h' - \tan\theta \right) + h' f_\eta^2$$

$$= \left( f_\eta f_{\eta\zeta} - f_\zeta f_{\eta\eta} \right) + \frac{1}{We} h^2 h'''. \tag{6}$$

Note that the above is merely a recasting of the standard shallow water equations in a coordinate system convenient to us. In the range of parameters of our interest, surface tension is found to be unimportant for the base flow, and this term is omitted for most of the discussion in this section. With $\theta$ set to 0, we recover the BLSWE describing horizontal film flow, in the coordinate system of Ref. 16. The zero velocity and the tangential stress balance, to $O(h')$, at the interface yield

$$f(0, \zeta) = 0, \quad f_\eta(0, \zeta) = 0, \quad f_{\eta\eta}(1, \zeta) = 0. \tag{7}$$

Note that the slope $h'$ of the film surface is an unknown quantity *a priori*. For a given *Fr* it is determined by imposing the additional constraint of mass flow conservation, derived from Eq. (3):

$$f(1, \zeta) = 1. \tag{8}$$

The height of a typical film flow, and therefore its Froude number, evolves as it progresses downstream. The streamwise component of the acceleration due to gravity acts to thin the sheet, and this is countered by viscous effects which slow it down and thicken it. Equations (6)–(8) can thus support, in the limit $h'Re \rightarrow 0$, a solution of constant height $h_p$. The subscript *p* indicates a parallel flow. The standardly used parabolic velocity profile,

$$f_\eta = 3\eta(1 - \frac{\eta}{2}) \tag{9}$$

arises in this limit. The corresponding constant Froude number $Fr_p$ depends only on the plate inclination and the Reynolds number, and is given by[5]

$$Fr_p^2 = \frac{1}{3} Re \tan\theta. \tag{10}$$

In the general case, $h' \neq 0$, and the size of the gravity term in Eq. (6) depends on the difference $h' - \tan\theta$. It is useful to define a non-dimensional number based on the slope of the film height, analogous to $Fr_p$, as

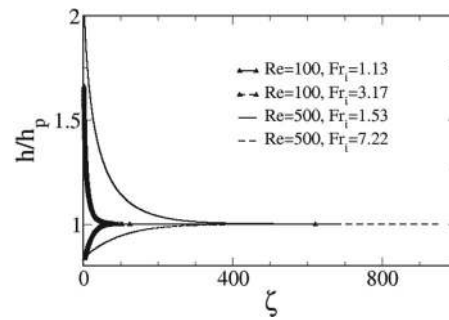$$S^2 \equiv \frac{1}{3} Re h'. \tag{11}$$

FIG. 1. The evolution of film height with downstream distance at an inclination of $10°$. The solid lines and solid symbols are for initial Froude number $Fr_i < Fr_p$, whereas the dashed lines and open symbols are for $Fr_i > Fr_p$.

As $Fr \rightarrow \infty$, Eq. (6) reduces to another known limit, that of Watson's gravity-free solution for film flow,[17] where $h'Re$ is known to take on a constant value of 1.8139 for any angle of inclination. We term $W \equiv 1.8139$ as the Watson constant. The gravity-free velocity profile is self-similar, since it is parameter-free, and satisfies

$$f_{\eta\eta\eta} + Wf_\eta^2 = 0. \tag{12}$$

For this Watson profile, we have $f_{\eta\eta}|_0 = 2.28$ at the wall. We now study the developing basic flow at finite Froude number.

Figure 1 shows one typical evolution of the height of the film as a function of downstream distance, for two Reynolds numbers. The method of solution is described in detail in Ref. 16. Briefly, beginning from an inlet Froude number $Fr_i$, a guess value for $h'Re$ is taken and iterated until the solution to Eq. (6) with $We = \infty$, subject to Eq. (7), satisfies Eq. (8). In this procedure, at each $x$ the terms on the right-hand side of Eq. (6) are evaluated, by solving the homogeneous equation at two locations separated by a very small amount. The procedure is then repeated for a non-zero right-hand side till its convergence. Using this value of $h'$ the computation marches downstream. Two points are obvious from this figure. One, that for this range of parameters, the flow evolves downstream to a constant height, irrespective of whether the inlet Froude number $Fr_i$ at $x = 0$ is greater than or less than $Fr_p$. We shall see below however that constant height is only achieved under SWT if both $Re$ and $Fr_i$ are above a certain $\theta$-dependent threshold. The second, and equally important, point is that the evolution to the final height takes a long downstream distance even when the initial heights are not too far from the parallel film height $h_p$. This is evident from Figure 1. Solutions at other angles of inclination give a similar picture, that it takes a very long downstream distance for the parabolic profile to be attained, even at modest Reynolds numbers. For example at a $3°$ inclination at $Re = 40$, the downstream distance at which the height reaches 99% of its final value is over a hundred times the initial thickness, for a starting Froude number of 10. At lower Reynolds numbers the developing region is even longer. In summary for $\theta = 3°$, we may say that if the starting Froude number is 2 or more, and the Reynolds number is 40 or lower, the length of the developing region is of the order of a hundred times the initial thickness. The local velocity profiles in this evolving flow, may often be visually only slightly different from parabolic, but this changes stability characteristics by a large amount, as will be seen below.

Figure 2 shows the slope of the film height as a function of Froude number for an inclination $\theta = 10°$. This information will help to classify the stability behaviour, and this figure therefore merits detailed discussion. A critical point is evident, with four branches around it. This point appears at first glance to be a saddle point, but is seen not to be a fixed point of the system, since $h' \neq 0$ there. The four branches are numbered in accordance with the quadrant in which they lie, with the critical point as origin. We first examine branches III and IV, beginning with the line of fixed points at $h'Re = 0$. This line corresponds to parabolic velocity profile solutions, with Reynolds number decreasing as we move from right to left. Consider the trajectory for a given Reynolds number, in the regime $W > h'Re > 0$ (the upper portion of branches III and IV). Since the height is increasing downstream, we have Froude number decreasing as a function of distance, i.e., the flow proceeds
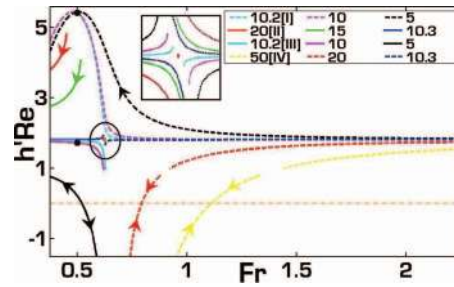
FIG. 2. $Reh'$ versus $Fr$ for various $Re$ at $\theta = 10°$. The legend gives the Reynolds number, and each row corresponds to a branch indicated in the square bracket in the first column. The critical point is shown by the data tip inside the inset. Arrows indicate the downstream direction. The horizontal dashed line intercepting the y-axis at zero corresponds to fixed points (parabolic solution) at different $Re$. The data-tips (outside the inset) show that two possible solutions at $Fr = 0.5$ at $Re = 10$. The Reynolds number decreases from bottom to top going from branch IV to branch I, and increases from bottom to top going from branch III to branch II. The inset shows a magnified qualitative image of the region around the critical point, indicated by the circle.

downstream from right to left in the figure. When $h'Re < 0$ on the other hand, flow proceeds from left to right. Branch IV solutions thus contain a stable fixed point at $h'Re = 0$. In other words, these solutions evolve towards a constant height profile irrespective of whether $Fr_i$ is higher or lower than $Fr_p$, so long as it occurs in branch IV. On the other hand, for branch III, from similar arguments we see that the constant height solution is an unstable fixed point, and solutions move away from it. Thus, according to SWT, only branch IV solutions will attain a parabolic profile, and this profile will be attained far downstream.

Moving upwards in Figure 2, we see that the trajectory at $h'Re = W$ behaves as a separatrix, with completely different behaviour on either side. At the separatrix, for $\theta = 10°$, $Re = W/\tan\theta = 10.28$ and we have a film of constant slope $W/Re$. Note that the constant term in Eq. (6) changes sign at this Reynolds number. When $Re < 10.28$, solutions lie on branches I and III, while solutions on the other branches occur at higher Reynolds numbers. Solutions on branches I and II evolve from right to left, not towards constant height, but to values not far from $h'Re = W$. Branch I solutions begin at high Froude, turn around at $Fr \sim 0.74$, go past a maximum in $h'Re$ and thereafter decrease monotonically, and seem similar to branch II in this graph, although their velocity profiles are very different.

We have thus far discussed the behaviour of solutions as we move up and down in Figure 2. We now discuss the left-right divide. To simplify the discussion, we recall that we have derived the BLSWE by retaining all terms *nominally* up to the first derivative in $\zeta$. However, the right-hand side is actually a higher order term, since for constant $h'$ we have a similarity solution. Departures from similarity, which the right-hand side is comprised of, emerge as a consequence of $h''$, and higher order variations in the film surface height. It is thus consistent with the shallow water assumption to reduce the BLSWE to

$$f_{\eta\eta\eta} - Re\frac{h' - \tan\theta}{Fr^2} + h'Ref_\eta^2 = 0, \tag{13}$$

which is an autonomous second order ordinary differential equation in $f_\eta$ that can be integrated to give

$$f_{\eta\eta}^2 - [f_{\eta\eta}|_0]^2 - Re\frac{2(h' - \tan\theta)f_\eta}{Fr^2} + h'Re\frac{2f_\eta^3}{3} = 0. \tag{14}$$

Mean flow computations for the entire range of our study confirm that the right-hand side does not change the answer noticeably. At an extremum $v_e$ in the velocity profile we have the cubic equation

$$v_e^3 - \frac{3\left[1 - \tan\theta/h'\right]}{Fr^2}v_e - \frac{3[f_{\eta\eta}|_0]^2}{2h'Re} = 0 \tag{15}$$

with a discriminant

$$\Delta = \frac{108}{Fr^6}\left[1 - \frac{\tan\theta}{h'}\right]^3 - \frac{243}{4}\frac{\left[f_{\eta\eta}|_0\right]^4}{(h'Re)^2}. \tag{16}$$

Only one real extremum is possible for negative $\Delta$, which means a monotonically increasing velocity profile. Reverse flow solutions, as they have multiple extrema, are only possible for non-negative $\Delta$. The $h'Re - Fr$ plane is broadly divided into left and right portions at the point where $\Delta$ crosses 0. For $h'Re = W$, and $\theta = 10°$, this corresponds to a critical Froude number $Fr_c = 0.74$, but the line dividing two kinds of behaviour in this case is a curved one, and is not a separatrix since flow trajectories do cross. When $Fr_i > Fr_c$, there is supercritical flow at the inlet, and depending on the Reynolds number, such solutions lie on either branch I or branch IV. On branches II and III there is subcritical flow at the inlet. The arguments above show that only attached velocity profiles with monotonically increasing velocity are possible to the right of $Fr_c$, while reverse flow solutions are possible below this Froude number. This is confirmed by the numerical solutions of both Eqs. (6) and (13). Branches II and III lie entirely below $Fr_c$ while branch IV lies above it, but branch I displays solutions for any $Fr$. Solutions on this branch begin with supercritcal $Fr_i$, and since $h'Re > 0$ always, $Fr$ is a monotonically decreasing function of the downstream coordinate $\zeta$. We note that branches IV and II, where $Re > W/\tan\theta$, can exist only for non-zero angles of inclination. On branch IV a short region is noticeable on some of the trajectories where the curves are not continuous. We were able to find no numerical solutions in this neighborhood, and the reasons for this are not clear at this time.

Close to $Fr = Fr_c$, branch I solutions display a relatively sharp change in $h'Re$, including a maximum in this quantity. Even at high Reynolds numbers, where $h'$ is small, the shallow water equations can sustain a singularity near this Froude number, as has been discussed in detail in the context of a horizontal plate in Ref. 18. We refrain from a repeat of that discussion here, but mention that hydraulic jumps may be displayed in this region. In this region the velocity profile on branch I changes from an attached one to a separated one.

Sample velocity profiles are shown in Figure 3. Since branch I solutions extend across the entire range of $Fr$, we may get multiple solutions for a given Froude number below $Fr_c$. The low Froude number regime is discussed briefly here, although it is not observed so far in direct simulations.

One example, at $Fr = 0.5$ is shown in the figure, with an attached velocity profile on branch III and a separated one on branch I. The former will be shown in Sec. III to be much more stable. A numerical search for multiple solutions was conducted for a wide range of Froude number and angles of inclination, for a wide range of initial guesses: $h'Re \equiv (-65, 65)$ and $f_{\eta\eta}(0) \equiv (-50, 50)$. Many examples of multiple solutions were found, and one case is shown in Figure 4. Among the four solutions shown, solutions 3 and 4 constitute the free surface moving counter to the mean flow.
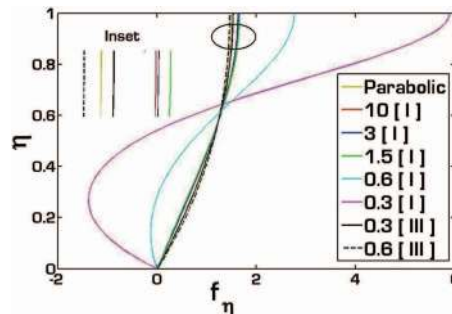


FIG. 3. Velocity profiles for $\theta = 4°$ and $Re = 10$ at various $Fr$. The legend gives the Froude number followed in parenthesis by the branch number. Velocity profiles with $h'Re < 0$, such as the branch III solution at $Fr = 0.6$, are seen to be fuller than parabolic. Solutions on branch I become less full as Froude number decreases, while those on branch III are closer to the parabolic profile but exhibit the opposite trend. The inset zooms the region around $f_\eta = 1.5$ and $\eta = 1$ to give a better view of the data. The lines shown in the inset correspond to the following flow conditions (from left to right): 0.6 [III], parabolic, 0.3 [III], 10 [I], 3 [I], and 1.5 [I]. Some numerical values characteristic of these profiles are provided in Table I.

TABLE I. The slope of the interface $h'$, and non-dimensional values of wall shear stress corresponding to the velocity profiles shown in Fig. 3.

| Branch | Froude | $h'$ | $f_{\eta\eta}$ |
|---|---|---|---|
| Parabolic | Any | 0.0 | 3.0 |
| I | 10.0 | 0.182002 | 2.27699 |
| I | 3.0 | 0.188676 | 2.24559 |
| I | 1.5 | 0.216829 | 2.10786 |
| I | 0.6 | 0.535966 | $-1.81030$ |
| I | 0.3 | 0.467401 | $-10.66376$ |
| III | 0.6 | $-0.082967$ | 3.26970 |
| III | 0.3 | 0.050001 | 2.82235 |

While finite regions of recirculation at the free surface are known in hydraulic jumps and in other situations, these solutions correspond to a very long streamwise region of recirculation, with no evident reattachment downstream. Thus, solutions 3 and 4 represent an entire layer at the surface moving upwards, counter to gravity, so these solutions seem unphysical. Second, a stability analysis shows that these solutions, as well as those which have a very large reverse flow region near the wall, are highly unstable, and are probably therefore not likely to be displayed in a real flow. This is in analogy with the highly separated solutions of Falkner-Skan equations, which are never seen. We therefore consider only solutions 1 and 2 as being valid profiles, belonging to branches I and III, respectively. In all the branches, the only physical solutions we obtained conformed to either of these types.

To estimate the effects of surface tension, we return to the base flow obtained, and calculate $h'''$ from it at each spatial location. Iterating for this quantity, we compute solutions including surface tension in the range $1 \leq Re \leq 500$, $0.2 < Fr < 100$, and $0 < \theta < 20°$. Using dimensional values corresponding to water, the Weber number may be estimated to lie in the range $10^{-4}$ to 10. Even for the smallest Weber number, the last term in Eq. (6) is observed to be only $\sim 10^{-3}$ relative to the largest term, so we conclude that surface tension effects are negligible in the base flow. Surface tension, however, is not negligible in the stability equation.

We conclude this subsection by noting that SWT predicts a richer solution structure than evidenced by prescribing a parabolic velocity profile.

## B. Numerical simulations

We supplement our study with a few numerical simulations, aimed at assessing the predictions of shallow water theory about the steady base flow. The simulations use a volume-of-fluid open source code, GERRIS.[19,20] Gerris employs a second order accurate staggered time discretization for the void-fraction and pressure fields and Godunov scheme for convective terms. A projection scheme
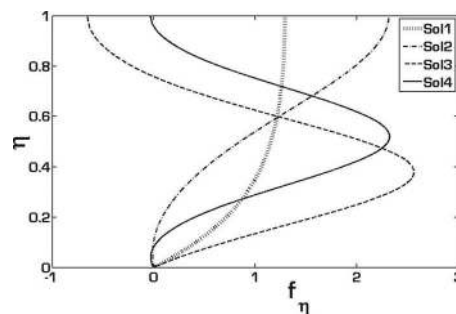


FIG. 4. Various streamwise velocity profiles satisfying Eq. (13) at $\theta = 0°$, $Re = 10$, and $Fr = 0.75$. Though multiple solutions are possible only one of them is seen to be an attached solution.
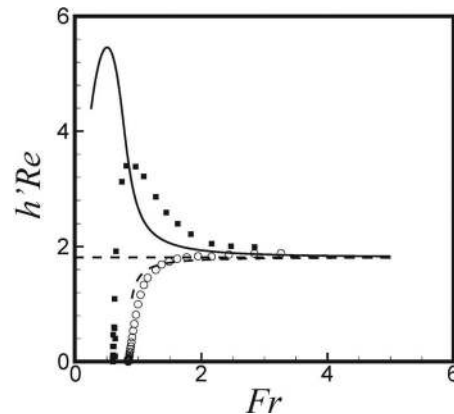
FIG. 5. The slope of the interface with respect to the inclined plate from SWT (lines) is compared to NSE (symbols). The solid line and solid symbols are at a Reynolds number of 20 while the dashed line and open symbols are at $Re = 40$.

is used to enforce the incompressibility condition ($\nabla \cdot \mathbf{u} = 0$). To capture the interface a Mixed-Youngs-Centred method for interface normal computation is employed, and a balanced-force surface tension calculation ensures low spurious currents at the interface. An adaptive mesh refinement is used through a quad/oct tree mesh. In the present simulations, the adaptive mesh refinement is performed by defining the vorticity and the gradient of the void-fraction field as the cost function. A detailed description of the numerical schemes is given in Ref. 19–21.

The computational domain and boundary conditions used are similar to those employed in Ref. 18. At the inlet, a half-parabolic velocity boundary condition is imposed and at the bottom surface of the computational domain, no-slip and no-penetration boundary conditions are imposed. To avoid the interference of the outflow boundary condition, essentially because of the effect of gravitational acceleration on a two-phase outflow, we design a pit near the exit through which the liquid flows out. The density ratio of the liquid and the surrounding air is $\rho_g/\rho_l = 0.01$ and the viscosity ratio is $\mu_h/\mu_l = 0.01$. Simulations have been performed for Reynolds number $Re = 5, 20$, and 40, and inlet Froude number $Fr = 0.1, 0.3, 10$, and 20. In the results presented here, we keep the angle of inclination fixed at $3°$.

As a first study, we wish to test the divide between branches I and IV. According to SWT, at $Re_s = W/\tan\theta$, which is 34.6 when $\theta = 3°$, there is a separatrix. Above $Re_s$ solutions lie on branch IV, and below it, they lie on branch I. We begin two simulations at high Froude number, and fix the two Reynolds number at 20 and 40, on either side of $Re_s$. The slope of the interface being very gentle, a plot comparing the height profiles is not very instructive. We instead plot the streamwise derivative of the height profile in terms of $h'Re$ as a function of the local Froude number, in Figure 5. Here the Froude number $Fr$, being equal to $Q^2/gh^3$, decreases as the downstream distance increases, and is an indirect measure of the same. We note that at high Froude numbers, the predictions from the NSE and SWT agree very well. Moreover, the split into branches I and IV for low and high Reynolds numbers, respectively, is evident. At a Froude number close to 1, SWT does not work too well, and the agreement between NSE and SWT is only qualitative. On the far downstream portion of the branch I solution (low $Fr$), we find that the NSE is able to cross the horizontal separatrix, unlike SWT, and drop down to a constant height solution. About the constant final height, decaying oscillations (not visible in this figure) are displayed over some streamwise distance.

It is important to note that the streamwise distance over which the film is developing is very long, of the order of 10 (for small $Fr_i$) to 100 (for higher $Fr_i$) times the initial thickness. This is the same as that predicted by SWT, so the profile is not parabolic for a very long streamwise distance. Thus numerical simulations too confirm the need to perform stability analysis for developing profiles. Moreover, numerical simulations also confirm that the streamwise development of the flow is very slow, even at modest Reynolds numbers, so both simulations and SWT indicate that a parallel flow assumption is a reasonable one. Shown in Figure 6 are a typical velocity profile and its
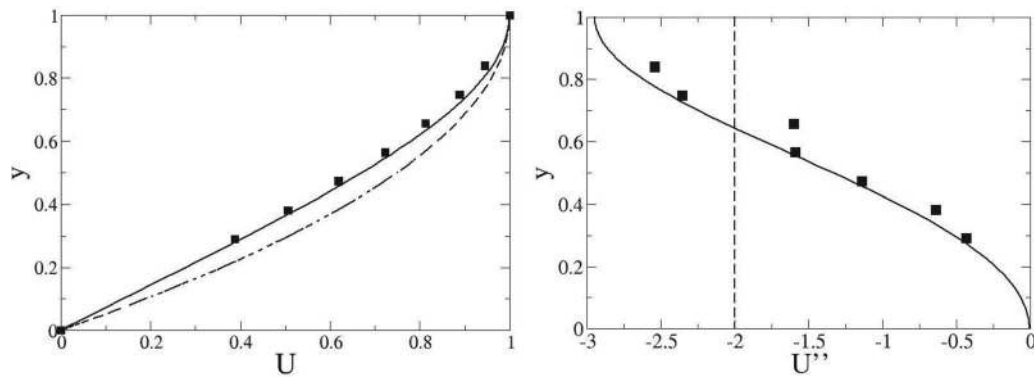
FIG. 6. Comparison of the velocity profile and its second derivative as predicted by SWT (solid lines) and simulations of the Navier-Stokes equation (symbols) at high Froude number, $Fr = 5.66$. The Reynolds number is 40. Shown by dashed lines are the parabolic velocity profile and its second derivative.

second derivative in this Froude number range. It is clear from the simulations, both that the profile here is not parabolic, and that SWT is sufficient to predict the basic flow in this Froude number range.

It is found to be not possible to perform numerical simulations for profiles starting on branch II. For branch III, the simulations do yield results, but of character different from the SWT. In particular, the initial slope of the $h'Re$ curve is highly negative, and the curve is able to cross to higher Froude numbers, where it spirals onto the stable node on $h'Re = 0$ at large downstream distance. Thus the simulations display one consistent trend which is fundamentally at variance with SWT. This is that the NSE does not respect the horizontal or vertical separatrix, and that at lower Froude numbers, after a long streamwise region of oscillations, the NSE ultimately settles down to a constant height solution of branch IV. Further work is needed to resolve this difference, and is beyond the scope of the present work.

## III. LINEAR STABILITY OF FILM FLOW ALONG AN INCLINED PLATE

Both shallow water theory and numerical simulations of the steady basic flow have indicated that film flow over an inclined plate most often does not attain a parabolic velocity profile for a long streamwise distance, and also that the streamwise development is slow. The latter observation means that the flow is only weakly non-parallel. In such flows, one may, as a first approximation, solve for the linear stability of a local velocity profile, i.e., one may make a "locally parallel flow" assumption. The assumption is not valid at Reynolds numbers of $O(1)$, where, if $h'Re \sim O(1)$, we have a significant streamwise development of the flow. Most of our study is therefore confined to $Re \geq 10$. We do present a few results at lower Reynolds numbers, and these are subject to correction by a complete global stability analysis, which is a subject of ongoing exploration.

Prescribing the perturbation streamfunction in normal mode form as $\psi(x, \eta, t) = \phi(\eta)e^{i\alpha(x-ct)}$, substituting in (2) and linearizing results in the Orr-Sommerfeld equation:

$$\phi'''' - 2\alpha^2\phi'' + \alpha^4\phi =$$
$$i\alpha Re\{(U - c)(\phi'' - \alpha^2\phi) - U''\phi\}. \tag{17}$$

Here $\alpha$ and $c$ are the streamwise wavenumber and phase speed of the disturbance mode, respectively, and the prime stands for differentiation with respect to $\eta$. With the perturbation film thickness denoted as $\kappa$, the kinematic, zero wall velocity, zero tangential stress and continuity of normal stress boundary
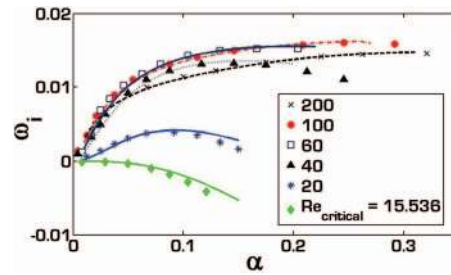
FIG. 7. Growth rate of the most unstable mode ($\omega_i$) as a function of wavenumber ($\alpha$) for a parabolic velocity profile at $\theta = 4.6°$ for various Reynolds numbers indicated in the legend. The Weber number corresponding to $Re_{critical}$ is 0.1, while the others scale suitably with $Re$. The data tips correspond to the data extracted from Fig. 2 of Ref. 9 while the lines correspond to the results for same flow conditions obtained by present approach. For the above curves, $\alpha$ corresponding to $\omega_{i,\,max}$ is seen to increase with $Re$.

conditions, respectively, are

$$\kappa = \frac{\phi(1)}{c - U(1)}, \tag{18}$$

$$\phi'(0) = 0, \phi(0) = 0, \tag{19}$$

$$\phi''(1) + (\alpha^2 + \frac{U''(1)}{c - U(1)})\phi(1) = 0, \tag{20}$$

$$\{\frac{\alpha Re}{Fr^2} + \alpha^3 WeRe\}\kappa + \alpha ReU'(1)\phi(1)$$
$$+\{(c - U(1))\alpha Re + 3i\alpha^2\}\phi'(1) - i\phi'''(1) = 0. \tag{21}$$

Equation (17) subjected to the boundary conditions (Eq. (18)–(21)) poses an eigenvalue problem, which is solved by Chebychev spectral collocation. When $\kappa$ is eliminated, the normal stress boundary condition (21) renders the eigenvalue problem nonlinear. This may be solved either directly as done by Ref. 9, or by trial and error, as we have done. Alternatively, a linear eigenvalue problem with an additional equation for $\kappa$ may be solved directly. This too has been done, and we have ensured that the results from the two approaches are the same. The latter method is far quicker. Figure 7 compares present solutions with the ones obtained by Ref. 9 for a parabolic mean profile, the agreement is very good. It is also ensured for $0 < \theta < \pi/2$ that for a parabolic velocity profile, the neutral stability Reynolds number, $Re_n$, agrees perfectly with the Yih[5] neutral Reynolds number:

$$Re_Y = 5/6 \cot\theta. \tag{22}$$

Yih's analysis was for long waves, but since the longest waves always become unstable first as a given parameter is changed, the neutral boundary is decided by long waves. From Eq. (10), it is evident that the above prediction is equivalent to stating that a parallel film flow is unstable at all Froude number above $Fr_Y \equiv 0.527$ for any angle of inclination. Moreover, the value of $Fr_Y$ places such a neutral location within branch III for all angles of inclination. In other words, when expressed in terms of a Froude number criterion, the parallel flow analysis only makes a statement about the neutral stability of a base flow which corresponds to an *unstable fixed point*. It is therefore clear that stability studies of the actual solutions of the BLSWE are in order. Another point to be noted is that while most earlier studies on film flow worked in the long wave limit, a parallel flow assumption is valid only when the basic flow does not change significantly over one wavelength of the perturbation. For a developing film, when $\alpha \sim h'$ or less, a parallel analysis may not suffice. Since $h'$ is small, this range is small too, but we must interpret our results at $\alpha \to 0$ with caution.
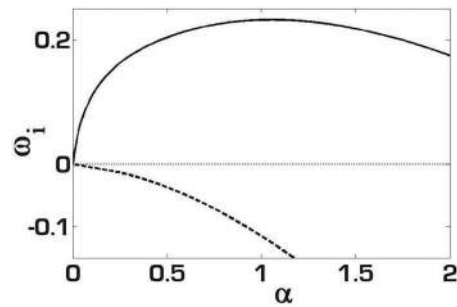
FIG. 8. $\omega_i$ versus $\alpha$ at $Fr = 0.5$, $Re = 10$, and $\theta = 4°$ for branches I (solid line) and III (dashed line) in the absence of surface tension.
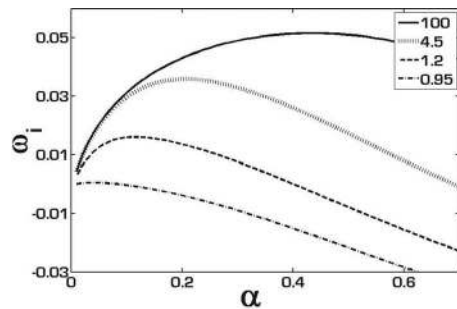


FIG. 9. $\omega_i$ versus $\alpha$ on branch IV at $Re = 50$ and inclination of $4°$ for various Froude numbers. For $Fr = 100$, $We = 1.23$, and the others are suitably scaled to hold the surface tension constant. The legend indicates the corresponding $Fr$.
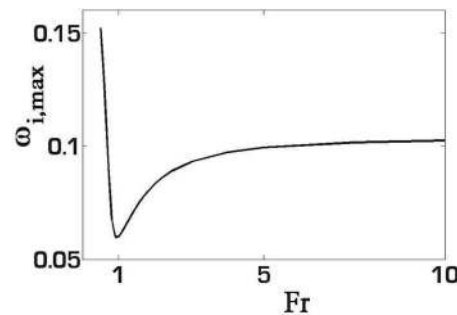


FIG. 10. $\omega_i$ as a function of Froude number for the branch I solution at $\theta = 4°$, $Re = 20$, and $We = \infty$.

Among these, we begin with the two base flow solutions highlighted in Fig. 2 at $Fr = 0.5$. The growth rates for the two are vastly different, as shown in Fig. 8. The branch III profile, being attached, is far more stable than the separated profile of branch I.

In Fig. 9, we follow a branch IV solution as the Froude number decreases, and plot the growth rate at various $Fr$ of the dominant disturbance mode as a function of wavenumber. Clearly the flow stabilizes as it evolves downstream, consistent with the observation that $h'$ decreases, so the velocity profile is fuller. The curve for $Fr = 0.95$ corresponds to a negative $h'$, where again the stabilisation is to be expected, given that the flow is accelerating. At $h' = 0$, the results at small $\alpha$ agree with the long wavelength predictions. It is relevant at this point to return to the experiments of Ref. 11, and point out that their conditions of $Fr$ and $Re$ may be calculated to lie within the regime of branch IV, and therefore the agreement of their experiments with traditional linear stability results is consistent with present predictions. In the initial phase of its evolution, the behaviour of the other supercritical case, namely branch I, is similar to branch IV. However, a turn-around is observed as displayed in Figure 10, followed by a dramatic increase in growth rate far downstream. This behaviour is to
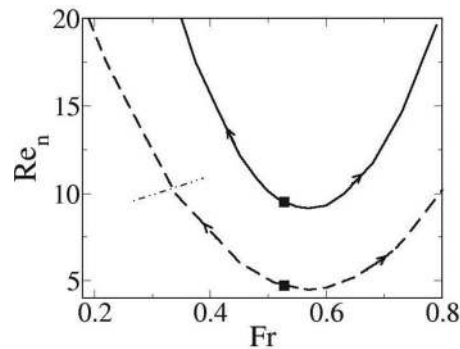
FIG. 11. Neutral stability boundary in the $Re$–$Fr$ plane for subcritical conditions for inclinations of $5°$ (solid line) and $10°$ (long dashes). The region above the curve is unstable. The solid squares show the Yih neutral point. For $\theta = 5°$, the curve lies entirely within branch III, while the cross-cutting line on $\theta = 10°$ shows the location above which the curve lies within branch II.
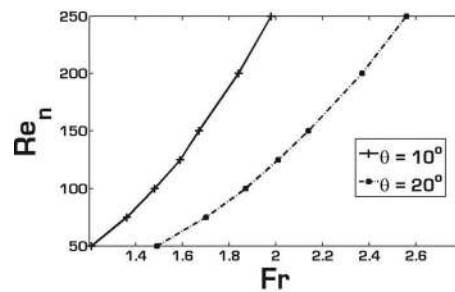


FIG. 12. Neutral stability boundary for supercritical conditions on branch IV. The region to the right of the boundary is unstable. Branch I solutions always lie to the right of the boundary and are always unstable as seen in Fig. 10.
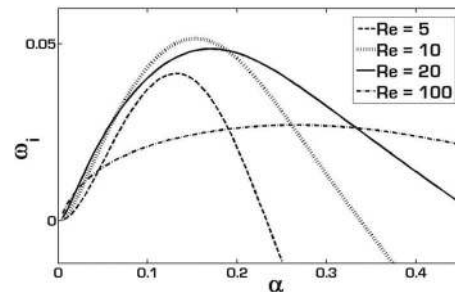


FIG. 13. $\omega_i$ versus $\alpha$ for branch I and IV solutions at $Fr = 4.5$ and $\theta = 4°$. We observe that the height of the peak does not monotonically increase with $Re$ but the $x$-intercept monotonically increases and thus the higher wavenumbers becomes unstable. This regime lies in branch IV, and as expected, the trend agrees qualitatively with that of Ref. 9 for a parabolic velocity profile. For the case $Re = 100$, $We = 0.393$, and surface tension is held constant across the curves.

be expected since below the critical Froude number, the flow on branch I separates, resulting in a recirculation bubble which increases in size as it moves downstream.

Figure 11 shows the neutral stability boundary for $\theta = 5°$ and $10°$ at subcritical conditions (branches II and III). There is a Reynolds number below which the flow is stable for subcritical Froude numbers. The neutral point of the Yih profile shown constitutes that of an unstable fixed point lying in branch III, and the arrows in the figure indicate the downstream direction. It is seen that whether the flow is accelerating ($Fr > Fr_Y$) or decelerating ($Fr < Fr_Y$), it becomes more and more stable as it progresses downstream.

For supercritical Froude numbers, branch I solutions are found to be unstable at all Reynolds numbers, while branch IV shows two kinds of behaviour. It is always unstable when the film is
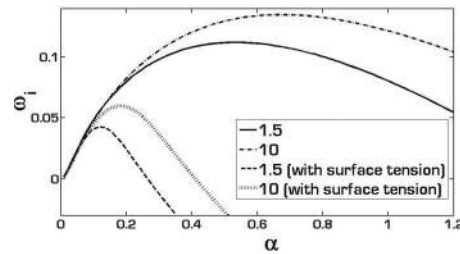
FIG. 14. The effect of surface tension on $\omega_i$ for branch I solutions at $Re = 10$ and $\theta = 10°$. The Froude number is indicated in the legend. For $Fr = 10$, $We = 0.03$, and for $Fr = 1.5$, $We = 0.009$.

decelerating $h' > 0$, but when the film is accelerating, a neutral boundary as shown in Fig. 12 is displayed. At a given Froude number, we see that higher Reynolds numbers are stable (Fig. 13), which may be contrasted with branch II and III solutions which are destabilized as the Reynolds number increases. Second, increasing the plate inclination is seen to stabilize branch IV, where branch III was destabilized by this. Note that earlier studies quote the neutral Reynolds number only at $Fr = 0.527$ for all $\theta$, and that flow is unstable at *higher* Reynolds numbers than the neutral. Thus earlier predictions of neutral location are restricted to the neighborhood of the unstable fixed point on branch III.

Some of the results which have been presented above are at finite $We$, and various realistic values, based on an water-air interface, have been imposed for this quantity. In all these cases surface tension, as expected, has a stabilizing effect on the shorter wavelengths, and has no effect on the longer waves. A direct comparison of stability with and without surface tension is shown in Fig. 14 to be along expected lines. Since long waves are not affected, the neutral boundaries shown above are independent of surface tension.

## IV. SUMMARY AND DISCUSSION

Film flows on inclined surfaces are often assumed to be of constant thickness, which ensures that the velocity profile is parabolic. Studying thin film flows under shallow water theory, we show that only "branch IV" flows, at a Reynolds number higher than $W/\tan\theta$ and Froude number $Fr_c$ higher than a critical $O(1)$ value can attain a constant thickness asymptotically as they progress downstream. A rich base flow structure is shown to exist in the $Re$–$Fr$ plane. When both $Re$ and $Fr$ are lower than their respective critical values (branch III), the constant height solution is shown to be an unstable fixed point, i.e., flows which begin with a constant height and half-Poiseuille velocity profile will evolve away from it as they move downstream. The traditional stability criterion prescribes that the neutral Froude number is 0.527 and all flows above this Froude are unstable. However, we show that this criterion pertains only to the unstable fixed points on branch III, where SWT predicts that constant film thickness profile cannot be maintained downstream. On branch II, $Re < W/\tan\theta$ and $Fr < Fr_c$. Finally, on branch I, with supercritical $Fr_i$, and $Re < W/\tan\theta$, flow proceeds towards subcritical Froude numbers and is analogous to the hydraulic jump regime of horizontal film flow. Simulations of the Navier-Stokes equations have been performed to obtain the base state. At high Froude numbers, the complete solutions agree very well with shallow water theory. At lower Froude numbers, either numerical solutions are not obtained, or when they are do not agree with SWT. It is interesting to note, however, that no constant height solution is obtained at Froude number below 0.7 or so. Numerical solutions begun at low Froude numbers cross over to higher Froude numbers before settling down to a constant height solutions.

Subcritical flows on branches II and III are shown to be unstable above a certain Reynolds number at a given Froude number, whereas supercritical accelerating flows on branch IV are unstable below a critical Reynolds number for a given $Fr$. Decelerating supercritical flows, whether on branch I or IV, are always unstable. A locally parallel assumption has been made in the present study. This is entirely consistent with the shallow water assumption of small slope of the film thickness. At large

plate inclinations, $W/\tan\theta$ is low, and the associated $h'$ is not small. In this regime, the shallow water theory must be called into question, and a basic flow computed by the complete Navier-Stokes equations, coupled with a global stability analysis must be performed. It is hoped that the present work will motivate stability experiments, and also more numerical simulations in the various regimes of $Fr-Re$ space described here.

## ACKNOWLEDGMENTS

[1] H. C. Chang and E. A. Demekhin, *Complex Wave Dynamics on Thin Films* (Elsevier Science, 2002).

[2] R. V. Craster and O. K. Matar, "Dynamics and stability of thin liquid films," Rev. Mod. Phys. **81**, 1131–1198 (2009).

[3] B. Ramaswamy, S. Chippada, and W. Joo, "A full-scale numerical study of interfacial instabilities in thin-film flows," J. Fluid Mech. **325**, 163–194 (1996).

[4] T. B. Benjamin, "Wave formation in a laminar flow down an inclined plane," J. Fluid Mech. **2**, 554–574 (1957).

[5] C. S. Yih, "Stability of liquid flow down an inclined plane," Phys. Fluids **6**, 321–334 (1963).

[6] F. W. Pierson and S. Whitaker, "Some theoretical and experimental observations of the wave structure of falling liquid films," Ind. Eng. Chem., Fundam. **16**(4), 401–408 (1977).

[7] Th. Prokoriou, M. Cheng, and H. C. Chang, "Long waves on inclined films at high Reynolds number," J. Fluid Mech. **222**, 665–691 (1991).

[8] R. W. Chin, F. H. Abernathy, and J. R. Bertschy, "Gravity and shear wave stability of free surface flows. Part 1. Numerical calculations," J. Fluid Mech. **168**, 501–513 (1986).

[9] L. Brevdo, P. Laure, F. Dias, and T. J. Bridges, "Linear pulse structure of signaling in a film flow on an inclined plane," J. Fluid Mech. **396**, 37–71 (1999).

[10] D. J. Benney, "Long waves in liquid film," J. Math. Phys. **45**, 150–155 (1966).

[11] J. Liu, J. D. Paul, and J. P. Gollub, "Measurements of the primary instabilities of film flows," J. Fluid Mech. **250**, 69–101 (1993).

[12] Yu. Ya. Trifonov, "Stability of wavy downflow of films calculated by the Navier-Stokes equations," J. Appl. Mech. Tech. Phys. **49**(2), 239–252 (2008).

[13] S. B. Singha, J. K. Bhattacharya, and A. K. Ray, "Hydraulic jump in one-dimensional flow," Eur. Phys. J. B **48**, 417 (2005).

[14] M. Amaouche, N. Mehidi, and N. Amatousse, "An accurate modeling of thin film flows down an incline for inertia dominated regimes," Euro. J. Mech. B/Fluids **24**, 4970 (2005).

[15] P. Bohorquez, "Competition between kinematic and dynamic waves in floods on steep slopes," J. Fluid Mech. **645**, 375–409 (2010).

[16] R. Dasgupta and R. Govindarajan, "Non-similar solutions of the viscous shallow water equations governing weak hydraulic jumps," Phys. Fluids **22**, 112108 (2010).

[17] E. J. Watson, "The radial spread of a liquid jet over a horizontal plate," J. Fluid Mech. **20**(Pt. 3), 481–499 (1964).

[18] R. Dasgupta, "A computational and semi-analytical study of laminar, standing hydraulic jumps," Ph.D. dissertation, Jawaharlal Nehru Centre for Advanced Scientific Research, Bangalore, 2011.

[19] S. Popinet, "Gerris: a tree-based adaptive solver for the incompressible Euler equation in complex geometries," J. Comput. Phys. **190**, 572–600 (2003).

[20] S. Popinet, "An accurate adaptive solver for surface-tension-driven interfacial flows," J. Comput. Phys. **228**, 5838–5868 (2009).

[21] G. Tomar, D. Fuster, S. Zaleski, and S. Popinet, "Multiscale simulations of primary atomization using Gerris," Comput. Fluids **39**(10), 1864–1874 (2010).